

## **Chapter 5**

# **Growth of high-quality AlGaN/(Al,Ga)N/GaN HEMTs using epitaxial AlN/sapphire templates as underlying substrates**

## **5.1. Introduction**

### **5.1.1. Foreword**

HEMTs based on AlGaN/GaN heterostructures are very promising electronic devices for high-power and high-frequency applications due to their superior material features, and their excellent performance has recently been demonstrated not only in high-power microwave devices but also in high-power and/or high-speed switching devices, as presented in Chapter 1. The recent progress in these devices has been sufficient to show that GaN and related alloys will play a significant role in the future development of high-power and high-frequency electronic devices.

Currently, sapphire has been widely used for the growth of GaN films. Although the low-temperature-buffer layer (LT-BL) technique [1-5] has reduced the effects of lattice mismatch between GaN and substrates, the defect densities in epitaxial films are still in the range of  $10^9$ - $10^{10}$  cm<sup>-2</sup>, which is on the order of one million times higher than in other semiconductor systems. These defect-laden materials, to date, have shown a surprisingly small effect on the performance of both optical and electronic devices, but they may raise major questions as to the long-term stability of these devices. It is predicted that high-crystal-quality epitaxial films are extremely required to obtain highly-reliable and high-performance electronic devices. On the other hand, our research group has shown that epitaxial AlN/sapphire

templates, which consist of epitaxial AlN films grown on sapphire at a temperature of higher than 1000°C, are very promising substrates for GaN epitaxial growth [6-8]. When AlN/sapphire templates are used as underlying substrates, overgrown GaN layers show higher crystal qualities than those grown on sapphire substrates using LT-BLs. It has also been reported that the device performance in GaN-based optical and electronic devices is improved by using epitaxial AlN/sapphire templates as underlying substrates [9-11]. We believe that this improvement is due to the high crystal quality of epitaxial films originating the crystal quality of the underlying epitaxial AlN films. In addition, we have recently developed a technology for growing epitaxial AlN films on 100-mm-diameter sapphire substrates. In this chapter, we have therefore attempted the MOVPE growth and characterization of AlGaIn/AlN/GaN [12,13] and AlGaIn/GaN HEMT structures on 100-mm-diameter epitaxial AlN/sapphire templates.

### **5.1.2. Epitaxial AlN/sapphire: A new underlying substrate for GaN Growth**

Our research group has shown that high-crystal-quality GaN films can be grown on epitaxial AlN/sapphire templates by MOVPE [8]. This section presents the features of epitaxial AlN/sapphire as a new underlying substrate for GaN growth.

Epitaxial AlN films are grown at a temperature of higher than 1000°C on *c*-face sapphire using a horizontal low-pressure MOVPE system [6,7]. Figure 5.1 shows an atomic force microscope (AFM) surface image for a 50-mm-diameter AlN/sapphire template [7]. As seen in this image, the AlN epitaxial film has an atomically flat surface with well-ordered atomic steps. The step height is measured to be approximately 0.2 nm, which corresponds to the AlN monolayer. Figure 5.2 shows the X-ray rocking curve (XRC) profiles for AlN (0002), (10-12) and (10-10) reflections [7]. Full widths at half maximum (FWHMs) of the XRC are approximately 80, 1450 and 1800 arcsec for (0002), (10-12) and (10-10) reflections, respectively. The total dislocation density of AlN films was estimated to be approximately  $1 \times 10^{10}/\text{cm}^2$  from transmission electron microscopy (TEM) observations [7].

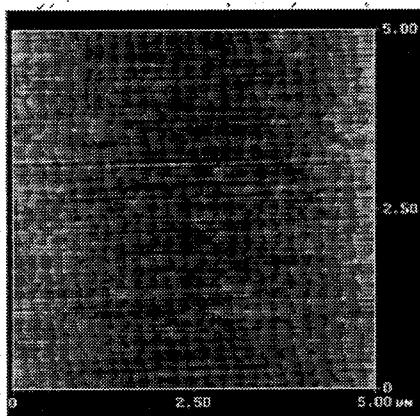


FIG. 5.1. AFM surface image of *c*-plane AlN grown on *c*-plane sapphire substrate for a scanning area of  $5\mu\text{m}\times 5\mu\text{m}$ .

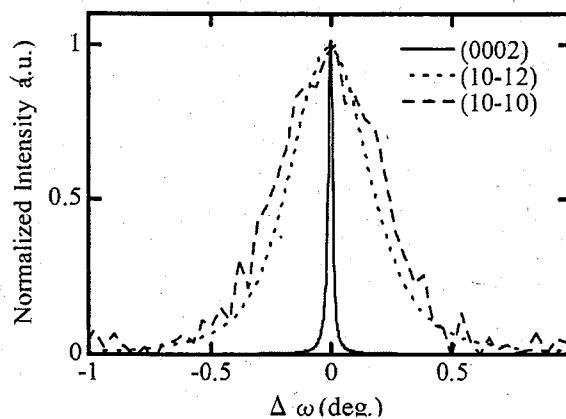


FIG. 5.2. XRC profiles of AlN epitaxial film for (0002), (10-12) and (10-10) planes.

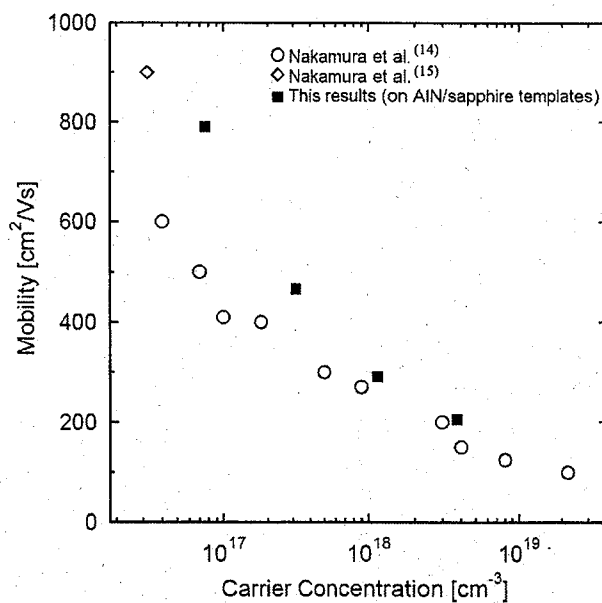


FIG. 5.3. Hall mobilities of MOVPE-grown GaN films as a function of the electron density.

We have also investigated the electrical and crystalline properties of MOVPE-grown GaN films on AlN/sapphire templates. Figure 5.3 shows the Hall mobilities of Si-doped GaN films grown on 50-mm-diameter AlN/sapphire templates as a function of the electron density at room temperature [8]. In this figure, the results for samples grown on sapphire substrates using LT-BLs reported by previous researchers [14,15] are also plotted. As seen in this figure, Hall mobilities of GaN films grown on AlN/sapphire are clearly higher than those of GaN films grown on sapphire with LT-BLs. High Hall mobilities of  $790 \text{ cm}^2/\text{V s}$  with an electron density of  $7.6 \times 10^{16}/\text{cm}^3$  at 300 K and  $1454 \text{ cm}^2/\text{Vs}$  with an electron density of  $1.8 \times 10^{16}/\text{cm}^3$  at 77 K were observed [8]. These mobilities are very high compared with previously reported values with the similar electron concentrations, as seen in Figure 5.3 [14,15]. Correspondingly, the crystal quality of GaN films grown on AlN/sapphire templates was found to be excellent. The XRC FWHMs are as small as approximately 60 arcsec for the (0004) reflection and approximately 230 arcsec for the (20-24) reflection compared with those of GaN films on sapphire substrates using LT-BLs (216 and 466 arcsec for (0004) and (20-24) reflections, respectively) [8]. Figures 5.4(a) and 5.4(b) shows AFM images of a GaN film grown on AlN/sapphire and on sapphire [8]. These figures clearly show that GaN films grown on AlN/sapphire exhibited a superior surface morphology compared with those grown on sapphire.

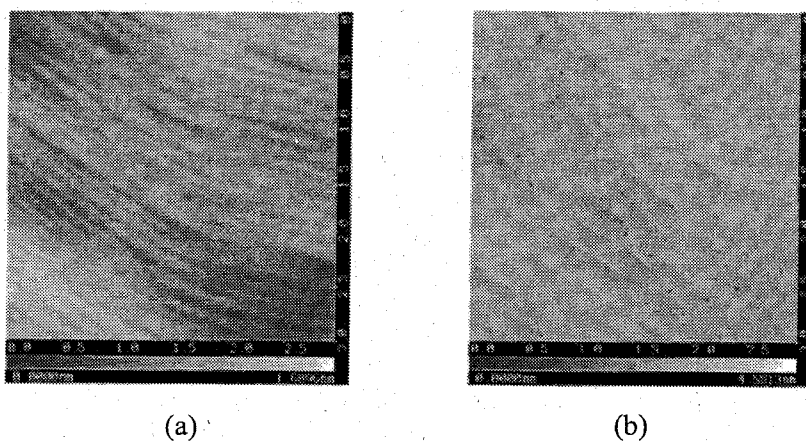


FIG. 5.4. AFM images of MOVPE-grown GaN films (a) on AlN/sapphire and (b) on sapphire for a scanning area of  $3 \mu\text{m} \times 3 \mu\text{m}$ .

Figure 5.5 shows a cross-sectional TEM image of an MOVPE-grown GaN film on an AlN/sapphire template [8]. From this image, the interface between the AlN and GaN layers is sharply observed. While dense dislocations (approximately  $1 \times 10^{10}/\text{cm}^2$ ) are observed in the underlying epitaxial AlN film layer, the dislocations did not thread to the GaN film layer. From the TEM observation, total dislocation density of the GaN film grown on AlN/sapphire templates was estimated to be approximately  $5 \times 10^7/\text{cm}^2$ . This value is one or more orders of magnitude lower than the previously reported values in MOVPE-grown GaN films on sapphire. From this, it can be expected that high-crystal quality GaN-based electronic devices are realized by using epitaxial films grown on AlN/sapphire templates.

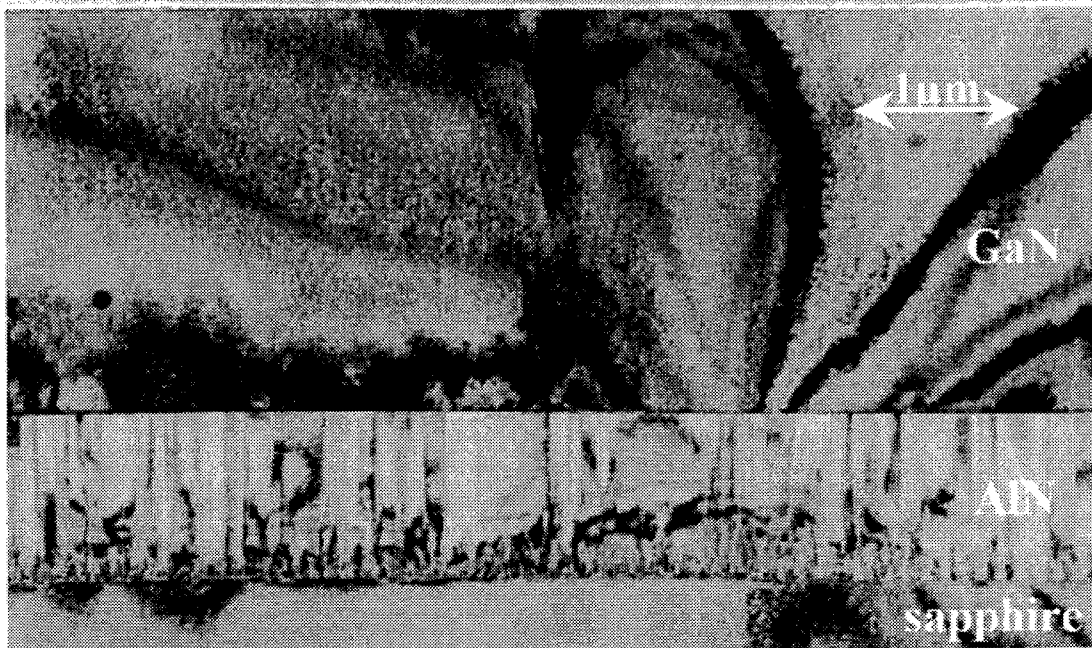


FIG. 5.5. Cross-sectional TEM image of a GaN film grown on AlN/sapphire.

## 5.2. Experiment

### 5.2.1. 100-mm-diameter epitaxial AlN/sapphire templates

1- $\mu\text{m}$ -thick epitaxial AlN films were grown at a high temperature ( $> 1000^\circ\text{C}$ ) on 100-mm-diameter and 630- $\mu\text{m}$ -thick *c*-face sapphire substrates using a home-made low-pressure MOVPE system [6,7]. XRD FWHMs for AlN (0002) reflections were less than 80 arcsec over the entire epitaxial wafer. Figure 5.6 shows a photograph of a 100-mm-diameter epitaxial AlN/sapphire template. As shown in Figure 5.6, a specular surface is successfully realized over the entire epitaxial wafer, and any irregular surface features such as micro-cracks have not been found from observation using Nomarski optical microscope. Figure 5.7 shows an AFM surface image of a 100-mm-diameter AlN/sapphire template. As seen in this image, the AlN epitaxial film has an atomically flat surface that atomic steps can be clearly observed. The surface roughness ( $r_a$ ) is less than 0.2 nm for a scanning area of  $5\ \mu\text{m} \times 5\ \mu\text{m}$ . The XRD and AFM results are approximately consistent with the previously results obtained for 50-mm-diameter AlN/sapphire templates [7].

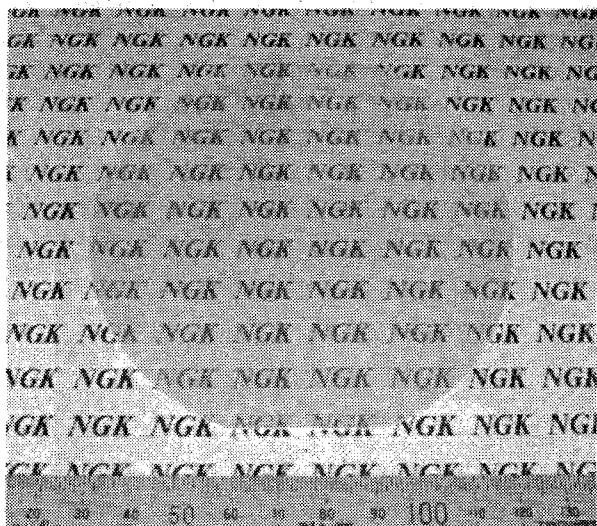


FIG. 5.6. Photograph of a 100-mm-diameter AlN/sapphire template.

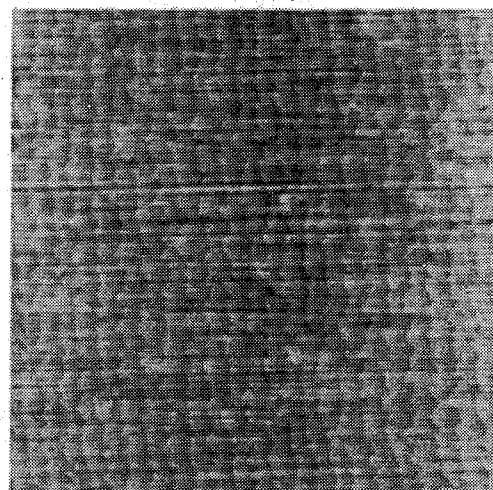


FIG. 5.7. AFM surface image (scan area:  $5\ \mu\text{m} \times 5\ \mu\text{m}$ .) of a 100-mm-diameter AlN/sapphire template.

The crystal quality of MOVPE-grown GaN films on 100-mm-diameter AlN/sapphire templates has also been confirmed. Figure 5.8 shows the in-wafer distributions of XRC FWHMs for (0004) and (20-24) reflections of GaN films grown on a 100-mm-diameter AlN/sapphire template and on a sapphire substrate. The XRC results showed that the sample grown on the AlN/sapphire template has excellent values of less than 100 and 300 arcsec for (0004) and (20-24) reflections, respectively, over the entire wafer compared with the sample grown on the sapphire substrate (> 200 arcsec and 500 arcsec for (0004) and (20-24) reflections, respectively). These XRC FWHM values are in almost agreement with the previously result obtained for 50-mm-diameter AlN/sapphire templates [8]. From this, it can be expected that large-diameter GaN-HEMT wafers with high crystal qualities are realized by using the 100-mm-diameter AlN/sapphire templates as underlying substrates.

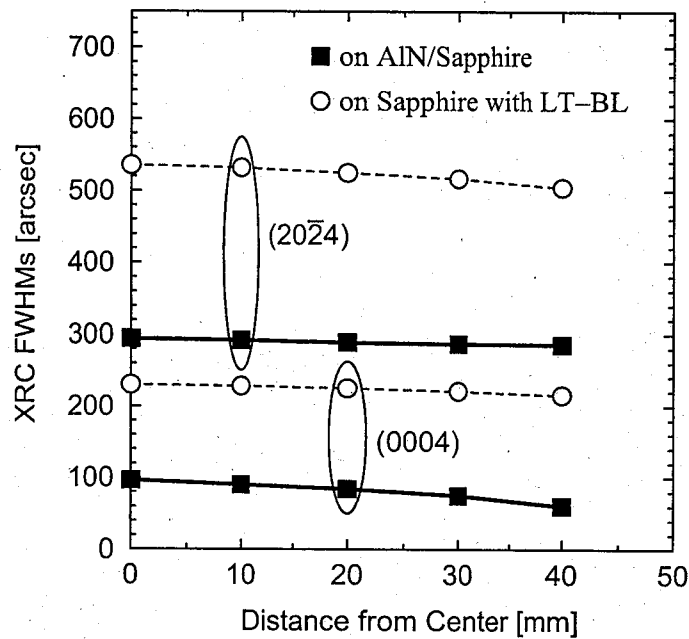


FIG. 5.8 In-wafer distribution of XRC FWHMs for GaN (0004) and (20-24) reflections grown on a 100-mm-diameter AlN/sapphire template and on a sapphire substrate.

### 5.2.2. Structures of MOVPE grown films and their characterization

Figure 5.9(a) schematically shows cross sections of the present MOVPE-grown samples. AlGaN/AlN/GaN and AlGaN/GaN structures were grown on epitaxial AlN/sapphire templates without any LT-BLs using horizontal MOVPE system (Taiyo Nippon Sanso, SR-4000). The AlGaN layer consists of, from top to bottom, a 3-nm-thick undoped  $\text{Al}_{0.26}\text{Ga}_{0.74}\text{N}$  layer, a 15-nm-thick Si-doped  $\text{Al}_{0.26}\text{Ga}_{0.74}\text{N}$  layer with the doping level of approximately  $5 \times 10^{18}/\text{cm}^3$  and a 7-nm-thick undoped  $\text{Al}_{0.26}\text{Ga}_{0.74}\text{N}$  layer. The thickness of the AlN interfacial layer in AlGaN/AlN/GaN structures was maintained at 1 nm. The AlGaN and thin AlN layers were grown on 2- $\mu\text{m}$ -thick highly insulating GaN (*i*-GaN) layers. For comparison, the AlGaN/AlN/GaN and AlGaN/GaN structures were also grown on 100-mm-diameter *c*-face sapphire substrates with 25-nm-thick GaN LT-BLs, as seen in Figure 5.9(b), in which the thickness of *i*-GaN layers was maintained at 3  $\mu\text{m}$ . The growth conditions of the *i*-GaN layers have been optimized to obtain a resistivity of higher than  $1 \times 10^6 \Omega\text{cm}$  over the entire epitaxial wafer. The MOVPE-grown wafers were characterized by XRD, TEM, AFM, Hall effect measurement and Hg-probe capacitance-voltage (*C-V*) measurement.

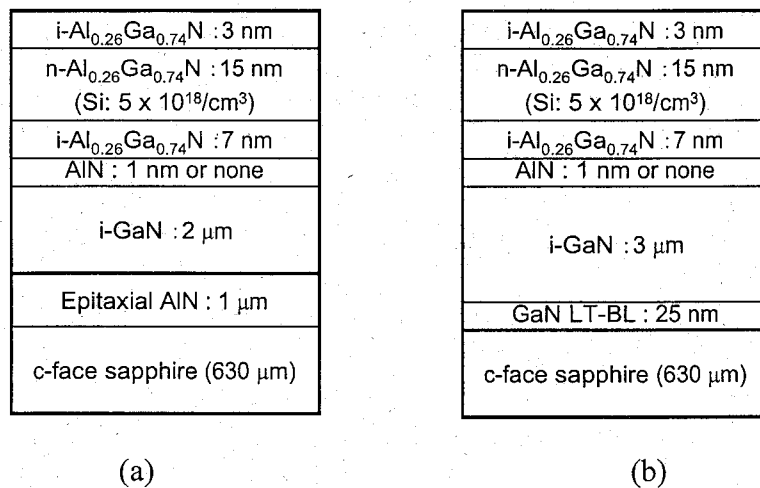


FIG. 5.9. Schematic cross section of MOVPE-grown samples on (a) AlN/sapphire template and on (b) sapphire substrate.

### 5.2.3. Fabrication of HEMTs and their characterization

The device fabrication was performed using a conventional photolithographic lift-off method. In this study, recessed ohmic contacts [16,17] were examined and compared with conventional nonrecessed ohmic contacts. Figure 5.10 shows the schematic cross section of the recessed ohmic HEMT. After ohmic lithography, recess etching was performed by  $\text{BCl}_3$  plasma reactive ion etching (RIE) using a parallel-plate reactor system. The etching conditions were as follows: 5 W input power, 10 sccm  $\text{BCl}_3$  flow, and 3 Pa pressure, which correspond to an etching rate of approximately 4 nm/min on an MOVPE-grown  $\text{Al}_{0.26}\text{Ga}_{0.74}\text{N}$  film. Source and drain patterns were then formed using self-aligned recesses and the evaporation of Ti/Al/Ni/Au (25/75/20/55 nm), and were subsequently annealed at a temperature of 850°C for 30 s in nitrogen atmosphere. The gate Schottky contacts were formed by the evaporation of Pd/Ti/Au (40/20/60 nm). Device isolation was accomplished by mesa dry etching down to *i*-GaN layers by RIE. Electron-beam-evaporated  $\text{SiO}_2$  films were used for device passivation. The gate width ( $W_g$ ) and the gate length ( $L_g$ ) were 15  $\mu\text{m}$  and 1.5  $\mu\text{m}$ , respectively. Current-voltage ( $I$ - $V$ ) characteristics were measured using a semiconductor parameter analyzer. Transmission line measurement (TLM) was used to investigate the ohmic contact resistance.

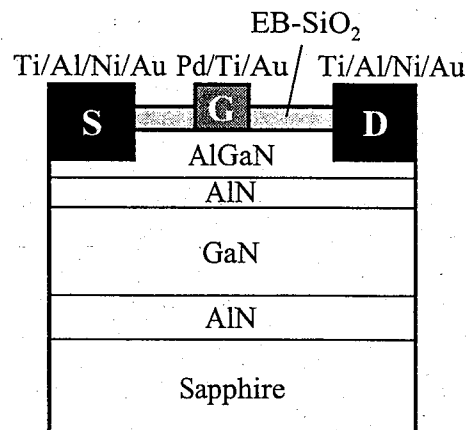


FIG. 5.10. Schematic cross section of the present recessed ohmic AlGaN/AIN/GaN HEMT.

## 5.3. Results and discussion

### 5.3.1. Electrical characterization of MOVPE-grown epilayers

Table 5.1 shows Hall mobility ( $\mu$ ), 2DEG density ( $n_s$ ) and sheet resistance ( $\rho_s$ ) measured at room temperature (RT) and at 77 K for AlGaN/AlN/GaN and AlGaN/GaN structures grown on AlN/sapphire templates and on sapphire substrates. From this table, it is clear that the Hall mobility markedly increases by using AlN/sapphire templates as underlying substrates. In particular, the AlGaN/AlN/GaN structure grown on AlN/sapphire showed the highest Hall mobility in this study. That is, 2174 cm<sup>2</sup>/Vs at RT and 17570 cm<sup>2</sup>/Vs at 77 K with a 2DEG density of approximately  $1 \times 10^{13}$ /cm<sup>2</sup>.

TABLE 5.1. Hall 2DEG density ( $n_{s\text{Hall}}$ ), Hall mobility ( $\mu_{\text{Hall}}$ ) and Hall sheet resistance ( $\rho_{s\text{Hall}}$ ) measured at room temperature and 77 K, and  $C$ - $V$  measured 2DEG density ( $n_{sC-V}$ ) values.

Structure	Substrate	$n_{s\text{Hall}}$ ( $\times 10^{13}$ /cm <sup>2</sup> )		$\mu_{\text{Hall}}$ (cm <sup>2</sup> /Vs)		$\rho_{s\text{Hall}}$ ( $\Omega$ /sq.)		$n_{sC-V}$ ( $\times 10^{13}$ /cm <sup>2</sup> )
		RT	77 K	RT	77 K	RT	77 K	RT
AlGaN/AlN/GaN	AlN/sapphire	0.95	0.95	2174	17570	302.2	37.4	0.98
AlGaN/GaN	AlN/sapphire	0.92	0.93	1420	4896	477.8	137.1	0.85
AlGaN/AlN/GaN	Sapphire	0.97	0.95	1770	7408	363.5	88.7	0.84
AlGaN/GaN	Sapphire	0.90	0.90	1287	3980	538.9	174.2	0.73

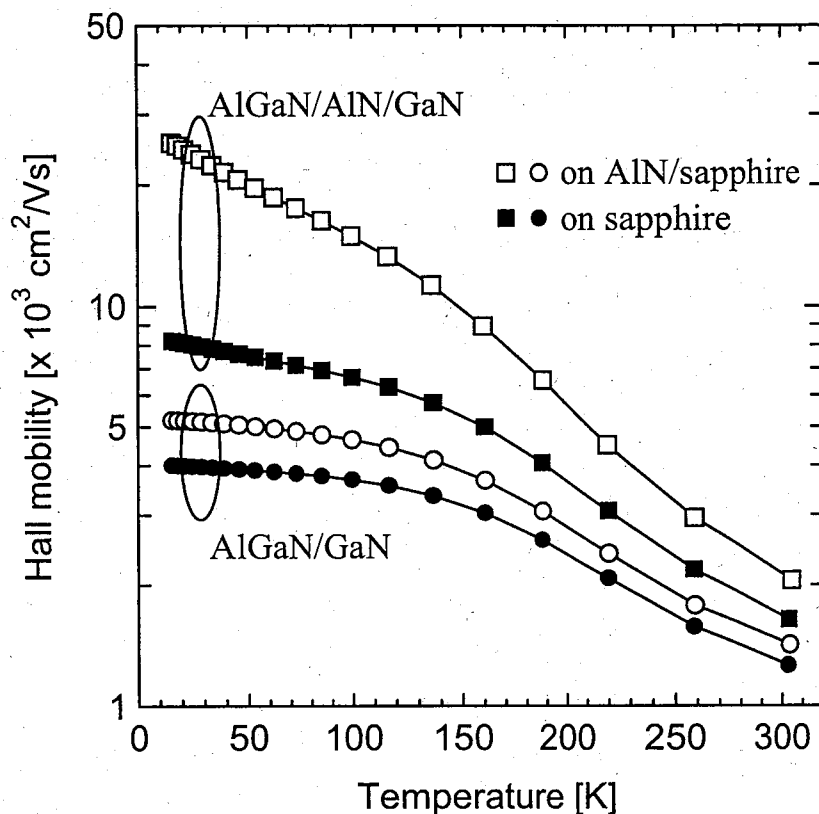


FIG. 5.11. Temperature dependence of Hall mobility for MOVPE-grown epitaxial wafers.

Figure 5.11 shows the temperature dependence of Hall mobilities for the MOVPE-grown epitaxial wafers. From this figure, the saturation of Hall mobilities at low temperatures, in which the alloy disorder and/or interface roughness is the dominant scattering process [18], is markedly reduced in the case of AlGaIn/AlN/GaN structures compared with that in the case of AlGaIn/GaN structures on both substrates. This result directly indicates that this dominant scattering process is largely reduced by the insertion of AlN interfacial layers. Figure 5.11 also shows that the low-temperature Hall mobilities of AlGaIn/AlN/GaN structures are significantly enhanced by the use of epitaxial AlN/sapphire templates as underlying substrates. The Hall

mobility of the AlGaN/AlN/GaN structure on an epitaxial AlN/sapphire template reaches a very high value of  $25500 \text{ cm}^2/\text{Vs}$  at 15 K. This is the highest value ever reported in the literature for MOVPE-grown AlGaN/GaN-based epitaxial films. Gaska *et al.* have reported a Hall mobility exceeding  $2000 \text{ cm}^2/\text{Vs}$  at RT and  $11000 \text{ cm}^2/\text{Vs}$  at 4.2 K with a 2DEG density of approximately  $1 \times 10^{13}/\text{cm}^2$  for AlGaN/GaN structures grown on 6H-SiC substrates [19]. Furthermore, it was confirmed that the 2DEG properties of the present AlGaN/AlN/GaN structure on the epitaxial AlN/sapphire template are in good uniformity over the entire 100-mm-diameter wafer (see Figure 5.12).

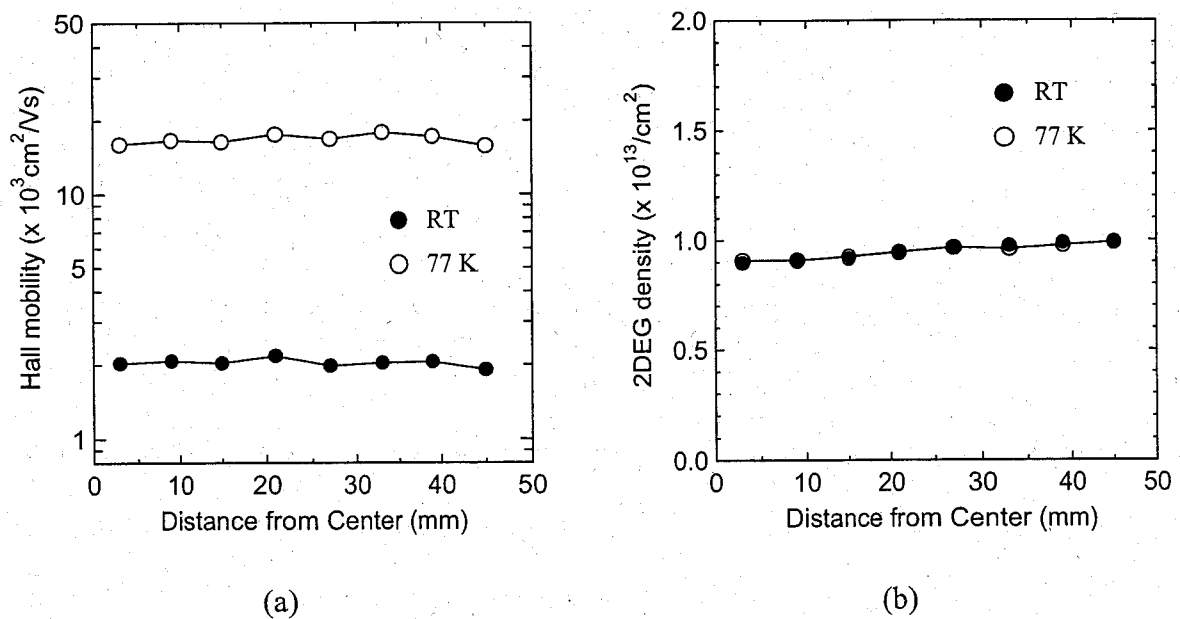


FIG. 5.12. In-wafer distributions of (a) Hall mobility and (b) 2DEG density for an AlGaN/AlN/GaN heterostructure grown on an epitaxial AlN/sapphire template.

Figure 5.13 shows typical results of  $C$ - $V$  profiling for MOVPE-grown epitaxial wafers. As seen in this figure, AlGaIn/AlN/GaN structures show a sharp 2DEG peak around the thin AlN interfacial layer with a 2DEG density of as high as  $1 \times 10^{20}/\text{cm}^3$ , while AlGaIn/GaN structures show a relatively broad 2DEG distribution and its penetration into the AlGaIn layer. The peak 2DEG density of AlGaIn/AlN/GaN structures was three to four times larger than that of AlGaIn/GaN heterostructures for samples on both substrates. This directly indicates that AlN interfacial layers enhanced the confinement of 2DEG in the GaN channel. The sheet 2DEG densities obtained by  $C$ - $V$  measurement ( $n_{sC-V}$ ) are also shown in Table 5.1. This result also showed that the thin AlN interfacial layer effectively suppresses carrier penetration into the AlGaIn layer and enhances the confinement of 2DEG in the GaN channel. We can consider that the well-confined 2DEG lead to high mobilities due to the suppression of alloy disorder scattering [12,13,18].

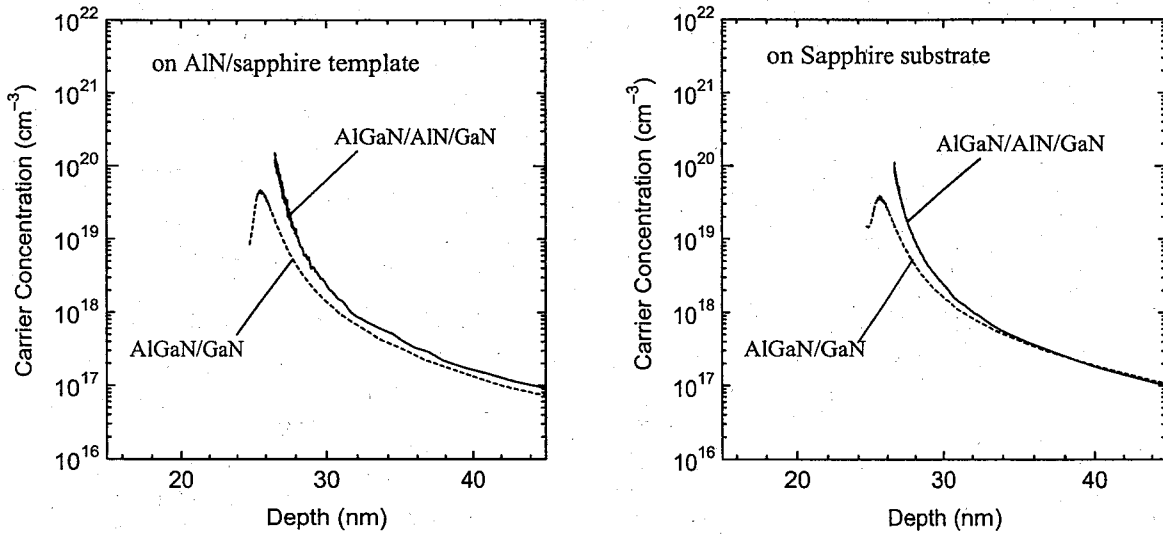


FIG. 5.13. Depth profiles of electron densities of AlGaIn/AlN/GaN and AlGaIn/GaN heterostructures grown on (a) epitaxial/AlN sapphire templates and on (b) sapphire substrates measured by the Hg-probe  $C$ - $V$  method.

### 5.3.2. Structural characterization of MOVPE-grown epilayers

Table 5.2 shows the dislocation densities in the GaN layers for MOVPE-grown samples. As seen in Table 5.2, the dislocation density in GaN films grown on AlN/sapphire is approximately one order of magnitude lower than that in GaN films grown on sapphire. This is in agreement with the previously reported result that the dislocation density in MOVPE-grown GaN films on AlN/sapphire is one or more orders of magnitude lower than that in GaN films grown on sapphire with a LT-BL [8].

TABLE 5.2. Dislocation densities in GaN layers and root-mean-square (RMS) surface roughness in AlGaIn layers for AlGaIn/AlN/GaN and AlGaIn/GaN structures grown on epitaxial AlN/sapphire templates and sapphire substrates.

Structure	Substrate	Dislocation Density in GaN ( $\text{cm}^{-2}$ )	RMS Roughness for AlGaIn (nm)
AlGaIn/AlN/GaN	AlN/sapphire	$2.5 \times 10^8$	0.12 – 0.16
AlGaIn/GaN	AlN/sapphire	$2.5 \times 10^8$	0.13 – 0.16
AlGaIn/AlN/GaN	Sapphire	$3.0 \times 10^9$	0.47 – 0.53
AlGaIn/GaN	Sapphire	$3.0 \times 10^9$	0.46 – 0.53

Figures 5.14(a) and 5.14(b) show the AFM surface images ( $1.0 \mu\text{m}^2$  scan area) of AlGaN/AlN/GaN films grown on an AlN/sapphire template and on a sapphire substrate, respectively. As seen in these figures, the surface of the sample grown on AlN/sapphire exhibits a clear step-like morphology compared with that of the sample grown on sapphire. The root-mean-square (RMS) surface roughness measured by AFM is also shown in Table 5.2. It is clear that the RMS roughness for samples grown on AlN/sapphire is much smaller than that for samples grown on sapphire. The present AFM results clearly indicate that AlN/sapphire templates improved the film quality not only of GaN layers but also of AlGaN layers on GaN layers.

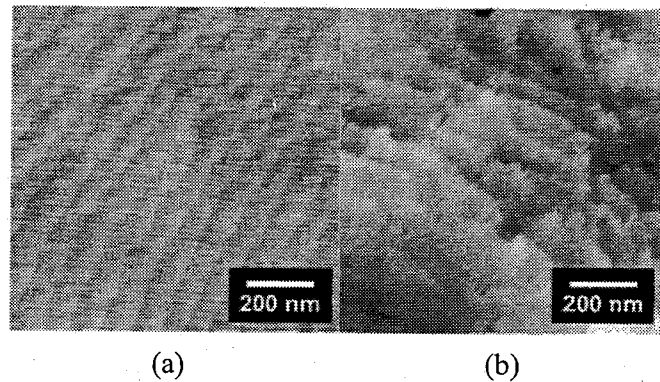


FIG. 5.14. AFM images ( $1 \mu\text{m} \times 1 \mu\text{m}$ ) of AlGaN surfaces for AlGaN/AlN/GaN heterostructures grown (a) on an epitaxial AlN/sapphire template and (b) on a sapphire substrate.

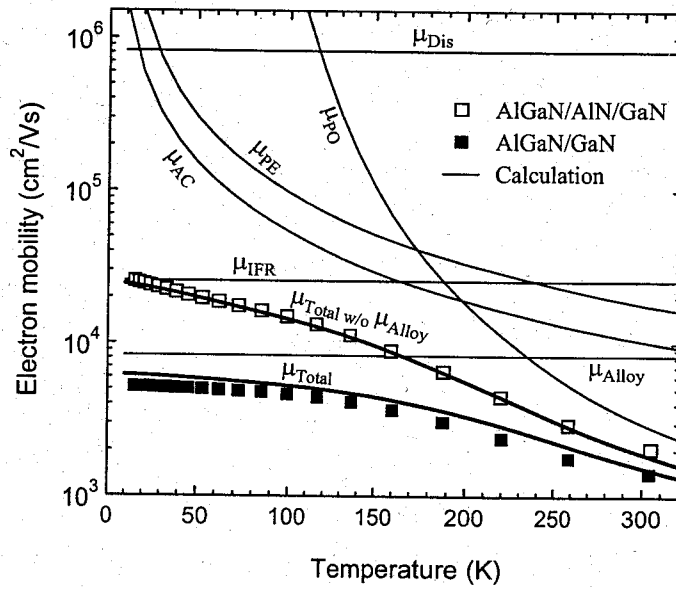
### 5.3.3. 2DEG transport properties of AlGaN/(Al, Ga)N/GaN structures grown on epitaxial AlN/sapphire templates

In order to understand the electron transport properties of 2DEG in MOVPE-grown samples, the carrier scattering mechanism was investigated in detail. Various kinds of carrier scattering processes, such as polar-optical phonons, acoustic phonons, piezoelectric field, alloy disorder, interface roughness and dislocation, were taken into account [20-22] according to the calculation presented in Chapter 3. The calculation was performed mainly using the parameters given in Ref. 20. The measured alloy composition and 2DEG density, shown in Tables 5.1 and 5.2, were also used as parameters.

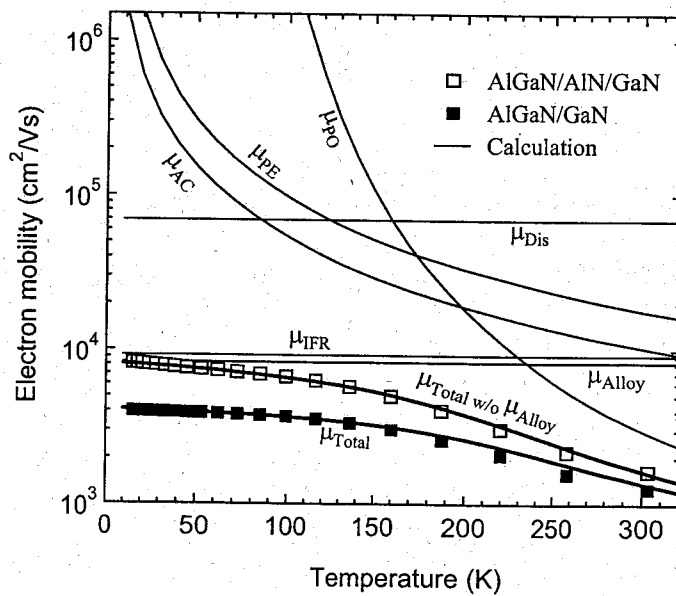
The differences in film qualities due to the underlying substrate, AlN/sapphire templates or sapphire substrates, were considered by adopting different parameters in the calculation of dislocation scattering and interface roughness scattering. Dislocation scattering was estimated [22] using the dislocation densities shown in Table 5.2. As a result, the mobility related to dislocation scattering ( $\mu_{\text{dis}}$ ) was calculated to be  $8.2 \times 10^5 \text{ cm}^2\text{V/s}$  for samples grown on AlN/sapphire templates. This calculated value is found to be one or more orders of magnitude higher than that for samples grown on sapphire substrates ( $\mu_{\text{dis}} = 6.9 \times 10^4 \text{ cm}^2\text{V/s}$ ). The mobility related to interface roughness scattering ( $\mu_{\text{IFR}}$ ) was characterized by fitting the calculated mobilities to the measured results using two parameters [22]: the root-mean-square roughness height ( $\Delta$ ) and the lateral correlation length ( $\Lambda$ ). The calculated results showed that samples grown on AlN/sapphire have a smooth interface ( $\Delta = 0.3 \text{ nm}$ ,  $\Lambda = 5.0 \text{ nm}$ ) and a high mobility ( $\mu_{\text{IFR}} = 2.6 \times 10^4 \text{ cm}^2\text{V/s}$ ) compared with samples grown on sapphire ( $\Delta = 0.5 \text{ nm}$ ,  $\Lambda = 5.0 \text{ nm}$ ,  $\mu_{\text{IFR}} = 9.2 \times 10^3 \text{ cm}^2\text{V/s}$ ). This result is in accordance with the present AFM results, which clearly show that samples grown on AlN/sapphire have a smooth surface morphology compared with those grown on sapphire. Thus, we theoretically confirmed that high-quality epitaxial films realized using AlN/sapphire templates can lead to high electron mobilities of

2DEG for AlGaN/GaN-based structures.

The other scattering processes were calculated assuming the same parameters for samples on both substrates, and the mobilities are combined according to the expression  $1/\mu = \sum_i (1/\mu_i)$ , where  $\mu_i$  represents an individual mobility. The calculated results for samples on AlN/sapphire and on sapphire are shown in Figures 5.15(a) and 5.15(b), respectively, in which the experimental results for AlGaN/GaN and AlGaN/AlN/GaN structures are also shown. As seen in these figures, the total mobilities ( $\mu_{\text{Total}}$ ), which mean the calculated values including all scattering processes, are in good agreement with the experimental results for conventional AlGaN/GaN structures grown on AlN/sapphire and on sapphire (solid squares in Figures 5.15(a) and 5.15(b), respectively). Also, we calculated total mobilities only excluding alloy disorder scattering. As a result, it was found that the calculated total mobilities excluding alloy disorder scattering ( $\mu_{\text{Total w/o } \mu_{\text{Alloy}}}$  in Figures 5.15(a) and 5.15(b)) are in good agreement with the experimental results for AlGaN/AlN/GaN structures on both substrates (white squares in Figures 5.15(a) and 5.15(b)). These agreements indicate that alloy disorder scattering has a strong impact on electron mobility in AlGaN/GaN structures and that the thin AlN interfacial layer effectively suppresses alloy disorder scattering to the extent that alloy disorder scattering can be neglected. This seems to be because the AlN interfacial layer enhances the confinement of 2DEG in the GaN channel [12,13,18]. We have also confirmed, from the  $C-V$  measurement, that the thin AlN interfacial layer effectively suppresses carrier penetration into AlGaN layers from the GaN channel.



(a)



(b)

FIG. 5.15. Temperature dependence of Hall mobilities in AlGaN/AlN/GaN ( $\square$ ) and AlGaN/GaN ( $\blacksquare$ ) heterostructures grown (a) on epitaxial AlN/sapphire templates and (b) on sapphire substrates, and calculated electron mobilities (solid lines) for polar-optical phonons ( $\mu_{PO}$ ), acoustic phonons ( $\mu_{AC}$ ), piezoelectric field ( $\mu_{PE}$ ), interface roughness ( $\mu_{IFR}$ ), dislocation ( $\mu_{Dis}$ ) and alloy disorder ( $\mu_{Alloy}$ ). The plots of  $\mu_{total}$  and  $\mu_{total}$  w/o  $\mu_{Alloy}$  represent combined mobilities including all scattering processes and combined mobilities only excluding alloy disorder scattering, respectively.

In the present calculation, the difference between underlying substrates was considered in the calculation of interface roughness and dislocation scattering, as explained above, and it has been confirmed that mobilities related to these scattering processes show much higher values for samples grown on AlN/sapphire substrates than those for samples grown on sapphire substrates. Therefore, very high mobilities obtained for AlGa<sub>N</sub>/AlN/GaN structures on AlN/sapphire templates can be explained by the high-quality GaN channel with a low dislocation density and a smooth interface, which was realized using AlN/sapphire templates as underlying substrates. We understand that the effect of AlN/sapphire templates has been clarified as a result of the reduction of alloy disorder scattering due to the insertion of a thin AlN interfacial layer.

#### **5.3.4. Fabrication of HEMTs and their characterization results**

HEMTs were successfully fabricated using the present MOVPE-grown epitaxial wafers. Figure 5.16 shows contact resistance ( $R_C$ ) for recessed ohmic AlGa<sub>N</sub>/AlN/GaN HEMTs grown on AlN/sapphire and on sapphire as a function of recess etching time. As seen in Figure 5.16, the  $R_C$  values decrease with etch depth up to an etching time of 6 min. The minimum  $R_C$  values of 0.51  $\Omega\text{mm}$  and 0.76  $\Omega\text{mm}$  were obtained for HEMTs on AlN/sapphire and on sapphire, respectively, at the etching time of 6 min, where the thicknesses of remained AlGa<sub>N</sub> layers were measured to be approximately 1 nm using AFM. This  $R_C$  reduction seems to be because the recessed ohmic structures enlarged the tunnelling current from the 2DEG in the GaN channel to the electrodes, which is reported to be a predominant carrier transport property for ohmic contacts in AlGa<sub>N</sub>/GaN HEMTs [16]. In addition,  $R_C$  values of samples on AlN/sapphire were found to be small compared with samples on sapphire, as seen in Figure 5.16. This seems to be because the defect density of AlGa<sub>N</sub> layers for samples on AlN/sapphire is low compared with that of AlGa<sub>N</sub> layers for samples on sapphire [9].

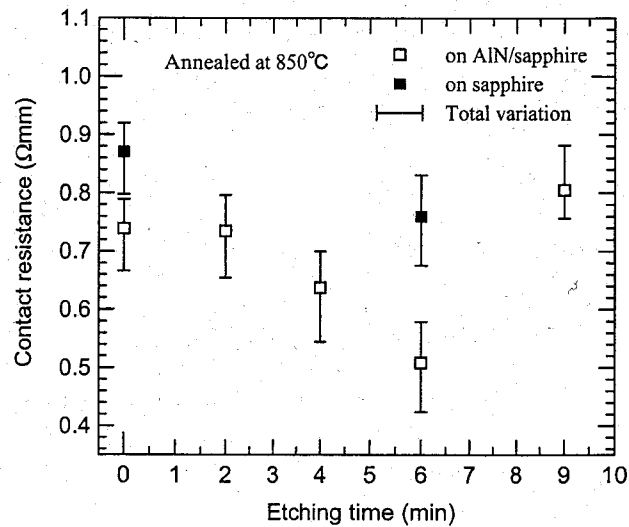
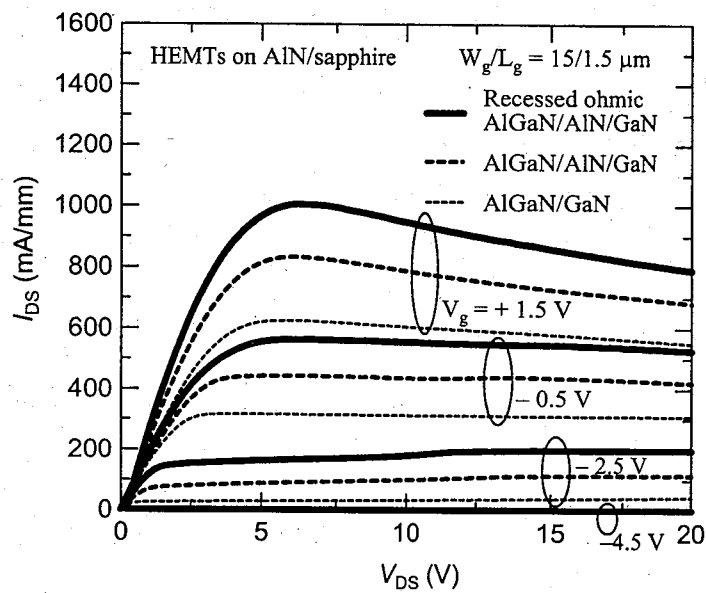
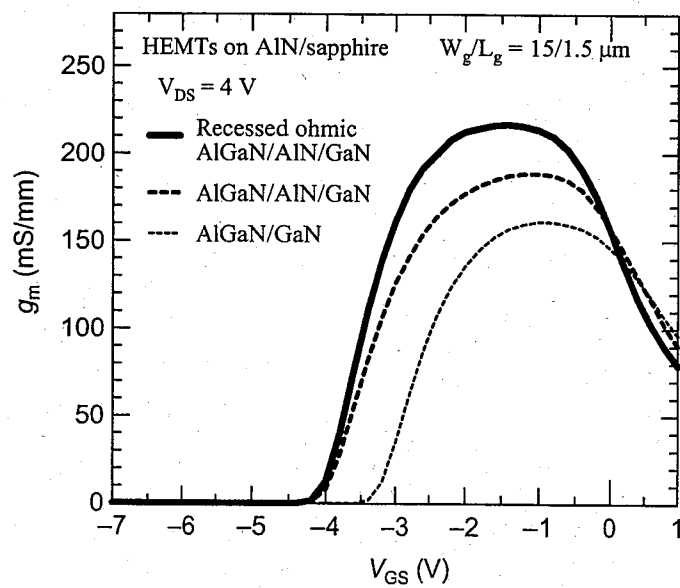


FIG. 5.16. Measured contact resistance ( $R_C$ ) in AlGaIn/AlIn/GaN HEMTs grown on AlN/sapphire and on a sapphire as a function of etching time for ohmic regions. Averaged contact resistances and total variations over 3-6 TLMs are shown.

Figures 5.17(a) and 5.17(b) show typical drain-source  $I-V$  characteristics ( $I_{DS}-V_{DS}$ ) and transfer characteristics ( $g_m-V_{GS}$ ), respectively, for AlGaIn/AlIn/GaN and AlGaIn/GaN HEMTs on AlN/sapphire templates. When comparing nonrecessed ohmic HEMTs, it is clear that AlGaIn/AlIn/GaN HEMTs showed better DC performances than those in conventional AlGaIn/GaN HEMTs. This seems to be because AlGaIn/AlIn/GaN structures have excellent 2DEG properties compared with conventional AlGaIn/GaN structures. Figures 5.17(a) and 5.17(b) also show the results of recessed ohmic AlGaIn/AlIn/GaN HEMTs. As seen in these figures, the DC performance of AlGaIn/AlIn/GaN HEMTs is clearly improved by applying recessed ohmic contacts. This seems to be due to the low  $R_c$  and  $R_s$  (source resistance) values obtained by applying recessed ohmic contacts. From this result, it was confirmed that recessed ohmic contacts are suitable for improving the device performance not only of AlGaIn/GaN HEMTs [16,17] but also of AlGaIn/AlIn/GaN HEMTs.



(a)



(b)

FIG. 5.17. Typical (a)  $I_{DS}$ - $V_{DS}$  characteristics and (b)  $g_m$ - $V_{GS}$  characteristics ( $V_{DS} = 4 \text{ V}$ ) of recessed and nonrecessed ohmic AlGaIn/AlN/GaN HEMTs and conventional AlGaIn/GaN HEMTs on epitaxial AlN/sapphire templates. The gate length ( $L_g$ ) and the gate width ( $W_g$ ) were  $1.5 \mu\text{m}$  and  $15 \mu\text{m}$ , respectively.

TABLE 5.3. DC characteristics in 1.5- $\mu\text{m}$ -gate-length recessed and nonrecessed ohmic HEMTs fabricated on the present MOVPE-grown epitaxial wafers.

Structure	Substrate	Ohmic contact structure	$R_S$ ( $\Omega\text{mm}$ )	$V_{th}$ (V)	$I_{DS\ max}$ (mA/mm)	$g_m\ max$ (mS/mm)
AlGaIn/AlN/GaN	AlN/sapphire	recessed	1.50	-4.08	1004	217
AlGaIn/AlN/GaN	AlN/sapphire	nonrecessed	2.00	-4.07	832	189
AlGaIn/GaN	AlN/sapphire	nonrecessed	2.48	-3.30	624	161
AlGaIn/AlN/GaN	Sapphire	recessed	2.04	-3.52	800	186
AlGaIn/AlN/GaN	Sapphire	nonrecessed	2.40	-3.49	712	170
AlGaIn/GaN	Sapphire	nonrecessed	3.24	-2.71	477	138

The DC characteristics of devices grown on AlN/sapphire templates and on sapphire substrates are summarized in Table 5.3. As seen in this table, changes in DC characteristics of HEMTs grown on sapphire due to the epilayer and ohmic contact structures showed almost the same tendencies with those in HEMTs grown on AlN/sapphire. In addition, it can be seen that samples grown on AlN/sapphire showed better properties than samples grown on sapphire. From this, it can be concluded that the electrical properties in MOVPE-grown GaN HEMTs are improved by using AlN/sapphire as underlying substrates. We can consider that this is due to the realization of high-crystal-quality GaN channel with good 2DEG properties. As a result, recessed ohmic AlGaIn/AlN/GaN HEMTs on AlN/sapphire showed the best performance in this study. A maximum drain current density ( $I_{DS\ max}$ ) of as high as 1004 mA/mm was observed with a low drain resistance ( $R_D$ ) of 3.51  $\Omega\text{mm}$  at a gate voltage of + 1.5 V for recessed ohmic AlGaIn/AlN/GaN HEMTs on AlN/sapphire. Correspondingly, a maximum extrinsic transconductance ( $g_m\ max$ ) of as high as 217 mS/mm was observed for recessed ohmic AlGaIn/AlN/GaN HEMTs on AlN/sapphire. On the other hand, it was observed that threshold voltage ( $V_{th}$ ) shifts by approximately 0.8 V toward a negative voltages with the insertion of a

1- $\mu\text{m}$ -thick AlN interfacial layer, as seen in Figures 5.17 and Table 5.3.  $V_{\text{th}}$  also shifts by approximately 0.6 V toward negative voltages using AlN/sapphire templates as substrates, which seems to be because the 2DEG for samples grown on AlN/sapphire templates is well confined in the GaN channel due to the realization of high crystal quality.

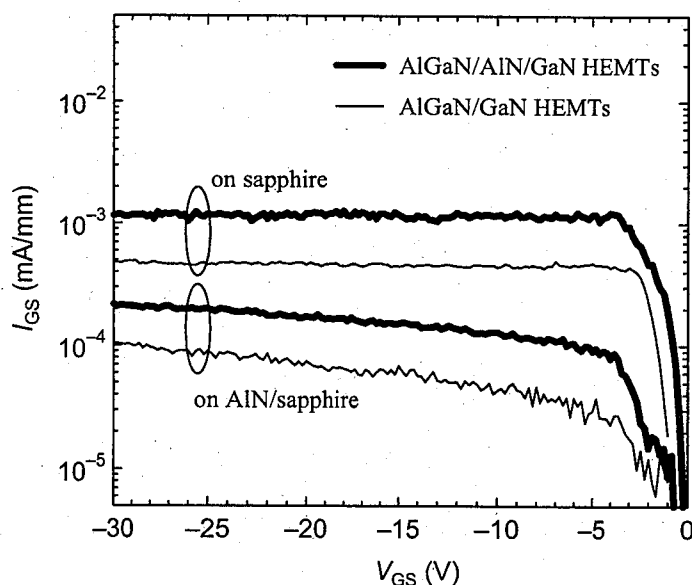


FIG. 5.18. Two-terminal gate-leakage characteristics ( $I_{\text{GS}}-V_{\text{GS}}$ ) of AlGaN/AlN/GaN and AlGaN/GaN HEMTs on AlN/sapphire and on sapphire.

Figure 5.18 shows the two-terminal gate-leakage current characteristics ( $I_{\text{GS}}-V_{\text{GS}}$ ) for AlGaN/AlN/GaN and AlGaN/GaN HEMTs on AlN/sapphire templates and on sapphire substrates. From Figure 5.18,  $I_{\text{GS}}$  for AlGaN/AlN/GaN HEMTs was observed to be approximately two times higher than that for conventional AlGaN/GaN HEMTs, for samples on both substrates. This may imply that a leakage current path was formed in AlGaN layers by the insertion of the thin AlN interfacial layer. On the other hand, it was found that  $I_{\text{GS}}$  decreases when AlN/sapphire templates are used as underlying substrates. In Figure 5.18,  $I_{\text{GS}}$

of samples grown on AlN/sapphire templates is seen to be approximately five times lower than that of samples grown on sapphire substrates when  $V_{GS}$  was applied up to  $-30$  V. This  $I_{GS}$  reduction seems to be due to the improved surface quality of AlGaIn layers. We believe that the leakage current of a Schottky contact for AlGaIn/GaN HEMTs is dependent on the surface quality of the AlGaIn layer (see Chapter 2). In addition, the present AFM study clearly revealed that samples grown on AlN/sapphire templates have better surface quality than that of samples grown on sapphire substrates (see Figure 5.14 and Table 5.2). Even though the insertion of the thin AlN interfacial layer increases the  $I_{GS}$  of AlGaIn/GaN-HEMTs, the use of AlN/sapphire templates as substrates can sufficiently compensate the  $I_{GS}$  increase.

## 5.4. Conclusion

In conclusion, we demonstrated the MOVPE growth and characterization of AlGaIn/AlN/GaN and AlGaIn/GaN structures on 100-mm-diameter epitaxial AlN/sapphire and sapphire substrates. It was found that a very high Hall mobility, such as  $2174$   $\text{cm}^2/\text{Vs}$  at RT and  $25500$   $\text{cm}^2/\text{Vs}$  at 15 K with a 2DEG density of approximately  $1 \times 10^{13}/\text{cm}^2$ , was uniformly obtained for the AlGaIn/AlN/GaN heterostructures on 100-mm-diameter epitaxial AlN/sapphire templates. Their structural and electron transport properties were also investigated in detail. The experimental and calculated results for 2DEG transport properties indicated that AlN/sapphire templates largely contribute to high electron mobility because they allow for the realization of a high-quality GaN channel with a low dislocation density and a smooth interface.

HEMTs were successfully fabricated and characterized. The fabricated devices showed good DC characteristics compared with those in devices grown on sapphire substrates. A high  $g_m$  max of approximately  $220$   $\text{mS/mm}$  and a high  $I_{DS}$  max of over  $1$   $\text{A/mm}$  were obtained for  $1.5$ - $\mu\text{m}$ -gate-length recessed ohmic AlGaIn/AlN/GaN HEMTs on AlN/sapphire templates. In addition, it was found that the use of AlN/sapphire templates is effective in reducing the gate

leakage current of nitride HEMTs. HEMTs based on AlGaN/AlN/GaN structures grown on epitaxial AlN/sapphire templates are very promising candidates for high-frequency electronic devices and/or high-efficiency switching devices and their applications.

## References

- [1] H. Amano, N. Sawaki, I. Akasaki, and Y. Toyoda, *Appl. Phys. Lett.* **48**, 353 (1986).
- [2] H. Amano, I. Akasaki, K. Hiramatsu, N. Koide, N. Sawaki, *Thin Solid Films* **163**, 415 (1988).
- [3] I. Akasaki, H. Amano, Y. Koide, K. Hiramatsu, N. Sawaki, *J. Cryst. Growth* **98**, 209 (1989).
- [4] S. Nakamura, *Jpn. J. Appl. Phys.* **30**, L1705 (1991).
- [5] S. Nakamura, M. Senoh, T. Mukai, *Jpn. J. Appl. Phys.* **30**, L1708 (1991).
- [6] T. Shibata, Y. Kida, H. Miyake, K. Hiramatsu, Y. Hori, K. Asai, T. Nagai, S. Sumiya, M. Tanaka, and O. Oda, *Compound Semiconductors 2001 (Inst. Phys. Conf. Ser. No. 170)*, 795 (2001).
- [7] T. Shibata, K. Asai, T. Nagai, S. Sumiya, M. Tanaka, O. Oda, H. Miyake, and K. Hiramatsu, *Mat. Res. Soc. Symp. Proc.* **693**, 541 (2002).
- [8] M. Sakai, H. Ishikawa, T. Egawa, T. Jimbo, M. Umeno, T. Shibata, K. Asai, S. Sumiya, Y. Kuraoka, M. Tanaka, and O. Oda, *J. Cryst. Growth* **244**, 6 (2002).
- [9] S. Arulkumaran, M. Sakai, T. Egawa, H. Ishikawa, T. Jimbo, T. Shibata, K. Asai, S. Sumiya, Y. Kuraoka, M. Tanaka, and O. Oda, *Appl. Phys. Lett.* **81**, 1131 (2002).
- [10] T. Egawa, H. Ohmura, H. Ishikawa, and T. Jimbo, *Appl. Phys. Lett.* **81**, 292 (2002).
- [11] B. Zhang, T. Egawa, H. Ishikawa, Y. Liu, and T. Jimbo, *J. Appl. Phys.* **95**, 3170 (2004).

- [12] I. P. Smorchkova, L. Chen, T. Mates, L. Shen and S. Heikman, B. Moran, S. Keller, S. P. DenBaars, J. S. Speck, and U. K. Mishra, *J. Appl. Phys.* **90**, 5196 (2001).
- [13] L. Shen, S. Heikman, B. Moran, R. Coffie, N. -Q. Zhang, D. Buttari, I. P. Smorchkova, S. Keller, S. P. DenBaars, and U. K. Mishra, *IEEE Trans. Electron Devices* **22**, 457 (2001).
- [14] S. Nakamura, G. Fasol, *The Blue Laser Diode*, Springer, Berlin 1997, p. 101.
- [15] S. Nakamura, *J. Appl. Phys.* **71**, 5543 (1992).
- [16] D. Qiao, L. S. Yu, L. Jia, P. M. Asbeck, S. S. Lau, and T. E. Haynes, *Appl. Phys. Lett.*, **80**, 992 (2002).
- [17] D. Buttari, A. Chini, G. Meneghesso, E. Zanoni, B. Moran, S. Heikman, N. Q. Zhang, L. Shen, R. Coffie, S. P. DenBaars and U. K. Mishra: *IEEE Electron Devices Lett.*, **23**, 76 (2002).
- [18] L. Hsu and W. Walukiewicz, *J. Appl. Phys.* **89**, 1783 (2001).
- [19] R. Gaska, M. S. Shur, A. D. Bykhovski, A. O. Orlov, and G. L. Snider, *Appl. Phys. Lett.* **74**, 287 (1999).
- [20] M. Shur, B. Gelmont, and M. A. Khan, *J. Electron. Mater.* **25**, 777 (1996).
- [21] L. Hsu and W. Walukiewicz, *Phys. Rev. B* **56**, 1520 (1997).
- [22] D. Zanato, S. Gokden, N. Balkan, B. K. Ridley, and W. J. Schaff, *Semicond. Sci. Technol.* **19**, 427 (2004).

## Chapter 6

### Conclusions

This dissertation has focused on the realization of high-quality and high-performance GaN HEMT epilayers on large-area substrates by MOVPE. Here, I summarized this dissertation as follows.

In Chapter 1, I reviewed the state-of-the-art of III-nitride semiconductors including growth technologies and devices. It was stated that GaN-based HEMTs are very promising electronic devices for high-power and high-frequency applications, due to their superior material features compared with those in other semiconductor materials. Some requisite technologies for the realization of GaN-based HEMTs were also presented.

In Chapter 2, I reported technologies for the uniform growth of AlGaN/GaN structures on large-area substrates by MOVPE. Different-Al-content AlGaN/GaN HEMT structures were successfully grown on 100-mm-diameter sapphire substrates under the optimized MOVPE growth conditions. It was confirmed that all of the HEMT layers showed specular surface morphology and have a good in-wafer structural uniformity. The results of electrical characterization also revealed a high homogeneity of MOVPE-grown AlGaN/GaN HEMT layers. HEMTs were fabricated and they exhibited good pinch-off properties. The dependence of the maximum drain current density on Al content was consistent with the Al-content dependence of 2DEG density. As a result, the maximum drain current density of 1033 mA/mm was obtained for 2- $\mu$ m-gate-length Al<sub>0.52</sub>Ga<sub>0.48</sub>N/GaN HEMTs. The uniformity of HEMTs DC characteristics were confirmed using devices fabricated at 40 locations on a

quarter of a 100-mm-diameter  $\text{Al}_{0.26}\text{Ga}_{0.74}\text{N}/\text{GaN}$  HEMT epiwafer. The uniformity of HEMTs DC characteristics were in good correlation with the electrical characteristics of  $\text{AlGaN}/\text{GaN}$  heterostructures, which was obtained from the Hall Effect and  $C$ - $V$  measurements.

In Chapter 3, I reported the detailed study on the structural and 2DEG transport properties in MOVPE-grown  $\text{AlGaN}/\text{GaN}$  heterostructures. Their alloy composition, layer thickness, tensile strain, in-plane stress, crystal quality and bandgap energy were determined in detail. The 2DEG properties of samples were theoretically as well as experimentally investigated taking into account the structural characterization results. It was confirmed that low-temperature 2DEG mobility largely decreases with the increase of the Al content. The theoretical calculation demonstrated that lower 2DEG mobilities in higher-Al-content samples are attributed to the poor interface quality at the  $\text{AlGaN}$  and  $\text{GaN}$  layers. This result is consistent with the experimental result that the surface of MOVPE-grown samples exhibited poor qualities with increasing Al content. It can be considered that the degradation of the surface and/or interface is associated with the strain-induced fluctuations at the  $\text{AlGaN}/\text{GaN}$  heterointerface, including structural and compositional fluctuations induced due to three-dimensional growth or partial relaxation.

In Chapter 4, I presented a study on mobility enhancement in modified  $\text{AlGaN}/\text{AlN}/\text{GaN}$  HEMT structures. It was confirmed that a high 2DEG mobility of  $1770 \text{ cm}^2/\text{Vs}$  and a low sheet resistance of  $365 \Omega/\text{sq.}$  with good in-wafer uniformity are obtained for a sample with an optimum  $\text{AlN}$  layer thickness of  $1.0 \text{ nm}$ . From the electrical uniformity of the MOVPE-grown samples, the  $\text{AlN}$  interfacial layer seemed to be uniformly grown on 100-mm-diameter wafers. Electron transport properties in  $\text{AlGaN}/\text{GaN}$  and  $\text{AlGaN}/\text{AlN}/\text{GaN}$  structures were theoretically studied. The calculated results demonstrated that the insertion of an  $\text{AlN}$  layer into the  $\text{AlGaN}/\text{GaN}$  heterointerface significantly enhances the 2DEG mobility due to the reduction of alloy disorder scattering to the extent that alloy disorder scattering can be neglected. HEMTs

were also fabricated and characterized. It was confirmed that AlGaN/AlN/GaN HEMTs show superior DC properties compared with conventional AlGaN/GaN HEMTs.

In Chapter 5, I presented the MOVPE growth and the characterization of AlGaN/GaN and AlGaN/AlN/GaN HEMT structures on 100-mm-diameter epitaxial AlN/sapphire templates. It was found that a very high Hall mobility, such as 2174 cm<sup>2</sup>/Vs at RT and 25500 cm<sup>2</sup>/Vs at 15 K with a 2DEG density of approximately  $1 \times 10^{13}/\text{cm}^2$ , was uniformly obtained for the AlGaN/AlN/GaN structures on epitaxial AlN/sapphire templates. Their structural and electron transport properties were investigated in detail. The experimental and calculated results for 2DEG transport properties indicated that AlN/sapphire templates largely contribute to the high electron mobility because they allow for the realization of a high-quality GaN channel with a low dislocation density and a smooth interface. HEMTs were also fabricated and characterized. The fabricated devices showed good DC characteristics compared with those in devices grown on sapphire substrates. A maximum extrinsic transconductance of as high as 220 mS/mm and a maximum drain current density of over 1 A/mm were obtained for 1.5- $\mu\text{m}$ -gate-length recessed ohmic AlGaN/AlN/GaN HEMTs on AlN/sapphire templates. In addition, it was found that the use of AlN/sapphire templates is effective in reducing the gate leakage current of GaN-based HEMTs. HEMTs based on AlGaN/AlN/GaN structures grown on epitaxial AlN/sapphire templates are very promising candidates for high-frequency electronic devices and/or high-efficiency switching devices and their applications.

I believe that these growth and characterization technologies will largely contribute to the future development of high power and high frequency electronic devices.